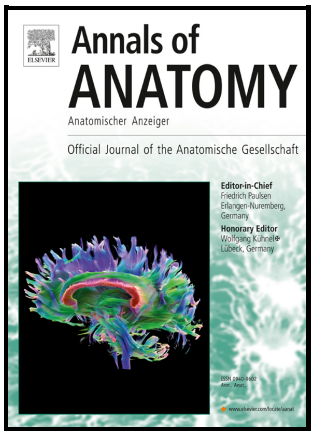

Mesoscopic 3D mapping and quantitative analysis of adult human dermal micro-vessels

Mulan Qahar, Shasha Li, Yan Shen, Jiawen Deng, Siwei Wang, Yi Ji, Yating Wei, Lijun Zhang, Hengyue Song, Jiangfen Li, Yongkang Zhu, Xiaoxi Li, Ilaria Dal Prà, Giovanna Orsini, Jie Xiao, Meishu Zhu, Guoqiang Bi, Guangtao Huang, Jun Wu

PII: S0940-9602(26)00583-2

DOI: https://doi.org/10.1016/j.aanat.2026.153362

Reference: AANAT153362

To appear in: *Annals of Anatomy*

Received date: 1 May 2026
Revised date: 4 August 2026
Accepted date: 18 August 2026

Please cite this article as: Mulan Qahar, Shasha Li, Yan Shen, Jiawen Deng, Siwei Wang, Yi Ji, Yating Wei, Lijun Zhang, Hengyue Song, Jiangfen Li, Yongkang Zhu, Xiaoxi Li, Ilaria Dal Prà, Giovanna Orsini, Jie Xiao, Meishu Zhu, Guoqiang Bi, Guangtao Huang and Jun Wu, Mesoscopic 3D mapping and quantitative analysis of adult human dermal micro-vessels, *Annals of Anatomy,* (2026) doi:https://doi.org/10.1016/j.aanat.2026.153362

Mesoscopic 3D mapping and quantitative analysis of adult human dermal micro-vessels

Mulan Qahar[1#], Shasha Li[1#], Yan Shen[#2], Jiawen Deng[1], Siwei Wang[3], Yi Ji[4], Yating Wei[1], Lijun Zhang[1], Hengyue Song[1], Jiangfen Li[1], Yongkang Zhu[1], Xiaoxi Li[1], Ilaria Dal Prà[5], Giovanna Orsini[6], Jie Xiao[1], Meishu Zhu[1], Guoqiang Bi[2,7,8*], Guangtao Huang[1*], Jun Wu[1*]

[1]Department of Burn and Plastic Surgery, Medical Innovation Technology Transformation Center, Shenzhen Second People's Hospital, The First Affiliated Hospital of Shenzhen University, Shenzhen 518035, China

[2]Interdisciplinary Center for Brain Information, The Brain Cognition and Brain Disease Institute, Shenzhen-Hong Kong Institute of Brain Science-Shenzhen Fundamental Research Institutions, Shenzhen Institutes of Advanced Technology, Chinese Academy of Sciences, Shenzhen 518055, Guangdong, China.

[3]Department of Dental Implantology, The Affiliated Stomatology Hospital of Zunyi Medical University, Zunyi, 563000, China

[4]Department of Burn and Plastic Surgery, Children's Hospital of Nanjing Medical University, Jiang Dong South Road, Nanjing, 210019, China

[5]Department of Surgery, Dentistry, Paediatrics and Gynaecology, University of Verona, 8 Strada Le Grazie, Verona, Venetia 37134, Italy

[6]Dipartimento di Scienze Cliniche Specialistiche e Odontostomatologiche, Università Politecnica delle Marche, Ancona, Marche, 60121, Italy

[7]Hefei National Research Center for Physical Sciences at the Microscale, Division of Life

Sciences and Medicine, University of Science and Technology of China, Hefei 230026, Anhui, China.

[8]Institute of Artificial Intelligence, Hefei Comprehensive National Science Center, Hefei 230088, Anhui, China.

[#]MQ, SL and YS are co-first authors.

*Correspondence to: Jun Wu, junwupro@126.com; Guangtao Huang, haitao3140@sina.com; Guoqiang Bi, gqbi@ustc.edu.cn

Abstract

The skin vascular plexus is essential to skin structure and function, with its morphological changes being linked to skin and systemic diseases. While current detection methods are largely limited to two-dimensional (2D) analysis, recent advances in tissue clearing and light-sheet imaging now enable three-dimensional (3D) visualization of microstructures, transforming this field. This study reports the first quantitative 3D histological analysis of adult human dermal microvascular system at a resolution of 1.0 μm. The results showed that the total length of blood vessels was 20.21 mm in 1 mm^3 of dermal tissue. The inner diameters of the papillary dermal plexus (PDP), superficial reticular plexus (SRP), and deep reticular plexus (DRP) were 0.23 to 8.41 μm, 0.01 to 44.43 μm, and 0.01 to 74.00 μm, respectively. Therefore, we calculated the total length of an adult's dermal blood vessels to be 36.4 to 181.9 km, and their total inner surface area to be 0.39-1.97 m^2. We estimated

the potential volume of dermal blood vessels, when fully opened and dilated, to be 412.0 ml. Interestingly, 48.99% of the dermal blood vessels were found to be closed. The vessels' branch numbers were assessed ranged from 25.53 to 56.20 in 1 mm^3 of dermal tissue, and from 0 to 265 for each vessel. The trajectories and angulations along the X, Y and Z axes of dermal vessels were measured as well. Our study investigated the quantitative 3D histological characteristics of human adult skin dermal vessels, which are relevant to histology, physiology, and pathology, as well as to tissue engineering.

Keywords

3D histology; Dermal microvascular system; Tissue clearing; Vascular plexus; Quantitative analysis

1. Introduction

As the largest organ enveloping the entire human body, the skin fulfils a multitude of physiological functions. These are prominently manifested in its unique barrier defense capabilities, sensorial reception, precise temperature regulation, limited yet vital absorptive activities, and the sweat and sebum glandular secretions. Skin vessels are essential for

maintaining these structures and functions. Particularly, they play crucial roles in nutrients transport, metabolic waste removal, and wound repair and regeneration, besides forming part of the human cardiovascular system, contributing to blood pressure regulation as well as keeping a blood fraction in reserve[1-4]. Damage to the structure and function of skin blood vessels can trigger or exacerbate various diseases, e.g., psoriasis, systemic lupus erythematosus, and hypertrophic scarring. Clinical symptoms often present with pronounced local manifestations, including erythema, edema, ulcers, purpura, abnormal thermoregulation, and paresthesia. In certain critical situations, the length and the volume of skin vessel plexuses are also relevant to patient resuscitation. Skin vascular diseases cause tissue damage and organ dysfunctions, which not only significantly impact patients' quality of life but can also endanger their lives. Moreover, alterations in the diameter and density of skin blood vessels can constitute early warning signs of cardiovascular and fibrotic diseases, providing invaluable diagnostic insights and therapeutic guidance for clinicians. Therefore, in-depth quantitative study of the skin blood vessel characteristics is of great significance for the prevention, diagnosis, and treatment of diseases.

Various methods have been used previously to reconstruct 3D images of skin vascular structures, such as histological staining, dermatoscopy, and optical coherence tomography. However, the 3D images reconstructed by these methods are not accurate and cannot be used to accurately measure vascular structures, because their information can only be inferred from fragmented 2D structures, which may be distorted due to folding, compression, or stretching of slices[5].

Currently, tissue transparency technology has been developed for the 3D imaging of tissue micro-structures[6-8]. This technique enables us to observe the tissue structures at the

mesoscopic level and to study the spatial relationships among microvessels, nerves, and cells, thereby providing a new perspective for the understanding of complex biological processes[9, 10]. In this study, we aimed to use this technique to display the spatial distribution of dermal blood vessels and to analyze their lengths, diameters and courses.

2. Material and Methods

2.1. Tissue preparation, imaging, and 3D reconstruction

All protocols were approved by the Ethics Committee of the First Affiliated Hospital of Shenzhen University (#2023-241-01PJ). A human skin sample was obtained from excess abdominal skin resected from a 38-year-old female patient (60 kg, 160 cm) during abdominoplasty. The sample was fixed in 4% HMS at 4°C for 12–16 h, washed in PBS, and cleared using a standard protocol[11]. Sample was immunostained with anti-CD31 antibody (1:200) and fluorescent secondary antibody (1:1000), counterstained with DAPI, and imaged using a light-sheet microscope implementing Volumetric Imaging with Synchronized on-the-fly-scan and Readout (VISoR) technology[12]. Raw images were processed for 3D volumetric reconstruction and output as IMS datasets[12].

2.2. Reconstruction and Identification of Vascular Networks in Human Skin

Images were acquired at a voxel resolution of 1 × 1 × 2.5 μm³. Vascular network reconstruction was performed semi−automatically using VISoR Suite (Bineogen Tech) and Lychnis (https://github.com/SMART-pipeline/Lychnis-tracing), supplemented by in−house MATLAB and Python scripts for enhanced precision and automation. Vascular structures in each skin tissue section were initially reconstructed by one human annotator, followed by dual‑round proofreading.

2.3. Tissue Thickness and Volume Measurements

Tissue thickness and volume were quantified along the z-axis from the reconstructed 3D image stacks. The upper and lower boundaries of the tissue were defined as the first and last z-planes that contained a continuous signal above a global intensity threshold. Overall tissue thickness (T) was calculated as the distance between these two boundaries.

$$T = z_{\max} - z_{\min}$$

The volume of each dermis layer (V_i) was determined from the number of voxels (n_i) contained within the segmented region, multiplied by the physical dimensions of a single voxel ($\Delta x \cdot \Delta y \cdot \Delta z$).

$$V_i = n_i \cdot \Delta x \cdot \Delta y \cdot \Delta z$$

2.4. Vessel Inner Diameters

The inner diameter (D_{inner}) was assessed using the VISoR Suite classifier, trained to identify the lumen region (e.g., by applying an intensity threshold or by CD31-positive endothelial labeling). The full width at half maximum (FWHM) was measured in cross-sections perpendicular to the centerline across the lumen and subsequently averaged. Let $D_{inner,i}$ be the inner diameter of the i-th cross-section:

$$D_{\text{inner}} = \frac{1}{n}\sum_{i=1}^{n} D_{\text{inner},i}$$

2.5. Vessel Counts

A single blood vessel was defined as a continuous network extending from a starting point through all branch paths to all endpoints. Connected SWC nodes were grouped to represent individual vessels, and the total number of such segments was recorded as the

vessel count. In the process of counting blood vessels at different dermal layers, a single vessel was sometimes artificially subdivided into multiple vessels (Fig. 9). Let V_i denote the i-th vessel segment and k the total number of segments. The vessel count (N) is given by:

$$N = \sum_{i=1}^{k} V_i$$

2.6. Vessel Lengths

The length of each vessel was calculated by summing the Euclidean distances between consecutive centerline nodes along the skeleton, based on SWC node parent–child relationships. Let (x_j, y_j, z_j) denote the coordinates of the j-th node along a vessel segment, and n the number of nodes in the segment. The vessel length (L) was computed as:

$$L = \sum_{j=1}^{n-1} \sqrt{(x_{j+1} - x_j)^2 + (y_{j+1} - y_j)^2 + (z_{j+1} - z_j)^2}$$

2.7. Vessel Branches and their Generation Points

Branch points were identified as SWC nodes connected to three or more neighboring nodes, indicating bifurcations or junctions. The total number of branches was quantified by systematically counting all such bifurcation points across the skeletonized dataset.

Our method for constructing a hierarchical vascular tree began with segmenting the vasculature from images using a pixel-wise classification model and creating a binary mask. From this mask, we extracted the vessel skeleton via morphological thinning to define the

centerline, while calculating the local vessel diameter by measuring the distance from the centerline to the vessel edges. The hierarchical structure was then established by analyzing all skeleton segments and designating the one with the largest average diameter as the first-level trunk of the vascular tree, thereby defining the primary branch from which all other branches were subsequently derived.

2.8. Vessel Segment Average Curvature

The average curvature of vessel segments was evaluated based on angular changes between successive segments along the path. For each node (x_j, y_j, z_j), the parent node $(x_{j-1}, y_{j-1}, z_{j-1})$ and grandparent node $(x_{j-2}, y_{j-2}, z_{j-2})$ were identified. Two consecutive vectors were computed:

$$v_1 = (x_{j-1} - x_{j-2}, y_{j-1} - y_{j-2}, z_{j-1} - z_{j-2})$$

$$v_2 = (x_j - x_{j-1}, y_j - y_{j-1}, z_j - z_{j-1})$$

The angle θ between vectors, representing local curvature, was calculated as:

$$\theta = \arccos\left(\frac{v_1 \cdot v_2}{|v_1| \cdot |v_2|}\right)$$

The average curvature over all N nodes was:

$$\text{AverageCurvature} = \frac{\sum \theta}{N}$$

2.9. Vascular Network Fractal Dimension

The fractal dimension of the network was computed using the box-counting method. The 3D coordinates of all nodes were extracted, and a bounding box encompassing all

nodes was defined. Grids of varying scales (e.g., $\epsilon = \text{box\_size}/2, \text{box\_size}/4, ...$) were applied. For each scale ϵ, the number of non-empty grids $N(\epsilon)$ containing nodes was counted. A linear regression was performed between $\log(N(\epsilon))$ and $\log(1/\epsilon)$, and the fractal dimension D_f was taken as the absolute slope of the fitted line:

$$D_f = \left|\frac{\Delta \log N(\epsilon)}{\Delta \log(1/\epsilon)}\right|$$

2.10. Vessels' Tortuosity

The morphological tortuosity of the cutaneous vascular network was quantified using a path-based computational approach. A root node was identified within the vascular graph as the origin. All terminal nodes—endpoints without downstream connections—were traced. For each terminal node i, the path length P_i was computed as the sum of segment lengths from the root to the terminal, and the Euclidean distance E_i was measured as the straight-line distance between the root and the terminal node. Tortuosity for each path was defined as the ratio P_i/E_i, and the mean tortuosity $\bar{\tau}$ was calculated as:

$$\bar{\tau} = \frac{1}{n}\sum_{i=1}^{n}\frac{P_i}{E_i}$$

2.11. Vessel Segments Orientation

The orientation of each vessel segment was determined from the direction vector between each SWC node and its parent. A right-handed Cartesian coordinate system was defined with the X-axis (left–right) and Z-axis (anterior–posterior) parallel to the skin surface, and the Y-axis perpendicular to it. For a segment between nodes (x_j, y_j, z_j) and $(x_{j+1}, y_{j+1}, z_{j+1})$, the direction vector was:

$$\vec{v} = (x_{j+1} - x_j, y_{j+1} - y_j, z_{j+1} - z_j)$$

The angle θ relative to a coordinate axis (e.g., the X-axis unit vector $\overrightarrow{e_x} = (1,0,0)$) was:

$$\theta = \arccos\left(\frac{\vec{v} \cdot \overrightarrow{e_x}}{|\vec{v}| \cdot |\overrightarrow{e_x}|}\right)$$

Angles were computed for all three axes and averaged across segments to characterize the overall orientation distribution.

2.12. Statistical analysis

All data analyses were performed using GraphPad Prism (version 10.12) and Microsoft Excel (version 2021). Violin plot data represent mean ± standard deviation (SD) values. Statistically significant differences were detected by one-way analysis of variance (ANOVA), and post hoc tests were performed with Bonferroni correction. The level of significance was set at $p < 0.05$.

3.Results

3.1. Human skin tissue made transparent via dDISCO-HMS technique

The dense and heterogeneous nature of mature human skin poses major hurdles to its volumetric imaging, chiefly because of intense light scattering, poor antibody accessibility, and profound structural collapse during lipid removal. While current tissue-clearing techniques perform well in neural or embryonic tissues, they often fail to preserve skin's structural integrity. To address this issue, we developed the dDISCO-HMS clearing strategy by combining dDISCO-based lipid extraction with hydrogel-based matrix stabilization (HMS). In this approach, a hydrogel monomer solution was infused into the

tissue and polymerized *in situ*, creating an internal scaffold that covalently anchored native biomolecules and mechanically supported the extracellular matrix. This critical step effectively locked the tissue into its original architecture, minimizing processing-induced deformations while enabling uniform antibody labeling **(Fig. 2a)**. By using light-sheet microscopy, we achieved a high-resolution ($1.0 \times 1.0 \times 2.5$ μm³) visualization of the entire dermal blood vessel network from the papillary layer to the deep reticular layer **(Fig. 2b, c)**. The resolution of 3D spatial images of the skin microvascular system could reach 1.0 μm[12] **(Fig. 2d)**. Our protocol further allowed a distortion-free reconstruction of full-thickness human skin sample, marking a substantial leap forward in quantitative analysis of skin microarchitecture.

3.2. Classification and localization of dermis anatomical layers

In this study, we measured a skin thickness of 5.25 mm, dimensions of 9.81 mm × 1.8 mm, and a volume of 92.72 mm³. All analyses of dermal vessels at various levels were separately conducted according to the established histological stratification, i.e., the papillary dermis, superficial reticular dermis, and deep reticular dermis **(Fig. 3a)**. In detail, the papillary dermal plexus (PDP) occupied the most superficial zone (to a depth of 0.35 mm) **(Fig. 3b; Table 1)**. The superficial reticular plexus (SRP) extended from the base of the papillary layer to a depth of 3.00 mm and was characterized by vertical communicating vessels **(Fig. 3c; Table 1)**. The deep reticular plexus (DRP) spanned from a depth of 3.00 mm to a depth of 5.25 mm, which corresponds to the dermal-subcutaneous boundary, and was identified by its horizontal orientation and integration with the subcutaneous vasculature **(Fig. 3d; Table 1)**.

Table 1. Layer-specific nomenclature and volumetric parameters of adult human dermis

Layers	Depth thickness (mm)	Volume (mm^3)
PDP	0.00-0.35	6.87
SRP	0.35-3.00	52.44
DRP	3.00-5.25	33.41

PDP, papillary dermal plexus; SRP, superficial reticular plexus;

DRP, deep reticular plexus.

3.3. The inner diameters of dermal blood vessels

The dimensional architecture of dermal blood vessels reflects their functional specialization across the different layers of the dermis. The vessel inner diameters exhibited considerable variations across the three dermal layers. The results showed that in the full-thickness dermis (FTD), 48.99% of the blood vessels had an inner diameter equal to 0.0 μm; hence, only 51.01% of the vessels were open **(Fig. 4)**. We further measured the blood vessel inner diameters across the three layers. In the PDP layer, 88.88% of blood vessel inner diameters were 0.0 μm, indicating their closed state, leaving only 11.12% open. In the SRP layer, 44.51% of the blood vessel inner diameters were 0.0 μm, while 55.49% of the vessels were open. In the DRP zone, 45.76% of blood vessel inner diameters were 0.0 μm; thus, 54.24% of them were open. Because these data were not normally distributed, we used median values. When excluding blood vessels with a diameter of 0.0 μm, vessel

inner diameters in FTD ranged from 0.01 to 74.00 μm (median, 3.45 μm), more specifically ranging from 0.23 to 8.41 μm (median, 2.8 μm) in PDP, from 0.01 to 44.43 μm (median, 3.45 μm) in SRP, and from 0.01 to 74.00 μm (median, 3.45 μm) in DRP **(Table 2)**. We further estimated the inner surface area (ISA) of the dermal blood vessels based on the total vessel length and inner diameter, according to the formula:

$S = \pi dh$,

where d is the median inner diameter of the vessel and h is the total vessel length in 1 mm^3 **(Table 3)**. In 1 mm^3 of FTD, the ISA was 0.219 mm^2. Therefore, assuming a typical adult human subject (height 170 cm, weight 70 kg, total skin surface area 1.8 m^2, and dermal thickness 1–5 mm), the total ISA of dermal blood vessels was to be 0.39 to 1.97 m^2. We further calculated the blood vessel ISA in the different dermal layers. If the blood vessels were fully dilated, the maximum measurable inner diameters of PDP, SRP and DRP would respectively be 8.41, 44.43 and 74 μm, respectively; therefore, the maximum ISA of the PDP, SRP and DRP layers would reach 0.40 m^2, 15.59 m^2 and 12.86 m^2, respectively.

Table 2. Vessels' inner diameters in the different dermal layers

Inner diameters (μm)	**Parameter**	**FTD**	**PDP**	**SRP**	**DRP**
Inner diameters = 0.0 μm	Fraction	48.99%	88.88%	44.51%	45.76%

Inner diameters (μm)	Parameter	FTD	PDP	SRP	DRP
Inner diameters > 0.0 μm	Fraction	51.01%	11.12%	55.49%	54.24%
	Median (μm)	3.45	2.8	3.45	3.45
	Range (μm)	0.01-74.00	0.23–8.41	0.01–44.43	0.01–74.00

FTD, full-thickness dermis; PDP, papillary dermal plexus; SRP, superficial reticular plexus; DRP, deep reticular plexus.

3.4. The length of dermal vessels

According to the methods we used for vessel counting and length measurement, there were 787 blood vessels found in 92.72 mm³ of dermal tissue, whose lengths ranged from 0.53 to 89.52 mm. The average length per vessel was 2.38 ± 6.17 mm (**Table 3; Fig. 5a**). The average total vessel length per 1 mm³ of dermal tissue was 20.21 mm **(Table 3)**. The courses of blood vessels were noted to differ **(Fig. 5a-f)**. We next conducted detailed measurements in the individual layers. There were 397 blood vessels in 1 mm³ of the PDP layer, whose lengths ranged from 0.03 to 3.62 mm with a total length of 24.17 mm. In 1 mm³ of the SRP layer, we detected 735 blood vessels, with lengths ranging from 0.02 to 53.71 mm and a total length of 23.43 mm. In 1 mm³ of the DRP layer, there were 260 blood

vessels, the lengths of which ranged from 0.05 to 16.32 mm with a total length of 13.67 mm (**Table 3**). Additionally, we measured the mean length of each blood vessel in the different dermal layers, i.e., 0.42 ± 0.50 mm at the PDP layer; 1.67 ± 4.14 mm at the SRP layer; and 1.76 ± 2.12 mm at the DRP layer (**Table 3**). Comparative analysis revealed that the average length of individual blood vessels in the PDP layer was significantly shorter than in the SRP and DRP layers ($p < 0.001$), whereas the difference between the SRP and DRP layers was not significant ($p = 0.9912$) **(Fig. 5b)**.

Accordingly, we could estimate the total blood vessel length inside 1 mm^3 of dermal tissue **(Table 3)** in adult human skin under the following conditions, i.e., a height of 170 cm, a weight of 70 kg, a body surface area of 1.8 m^2, and a dermal thickness of 1-5 mm using the following formula:

$$Total\ vessel\ length = body\ surface\ area \times dermal\ thickness \times vessel\ length\ per\ 1\ mm^3$$

Thus, the estimated total length of dermal blood vessels in a typical adult human ranged from 36.4 to 181.9 km.

We further estimated the dermal vessel volume (DVV) based on total vessel length and inner diameter. The DVV (v) was calculated as:

$$v = (\pi/4) \cdot d^2 \cdot h$$

where d is the median inner diameter of the vessels and h is their length. For an adult patient with a height of 170 cm, a weight of 70 kg, and a total skin surface area of 1.8 m^2, under general anesthesia (GA), 51% of the blood vessels were open, and the DVV-GA was approximately 0.8 ml. If the dermal blood vessels were supposed to be fully open and

dilated, the maximum measurable inner diameters of PDP, SRP and DRP were 8.41 μm, 44.43 μm and 74 μm, respectively, and therefore, the DVV-max was 412.0 ml.

Table 3. Vessels' lengths in different dermal areas

Parameter	**FTD**	**PDP**	**SRP**	**DRP**
Count	787	397	735	260
Length range (mm)	0.53-89.52	0.03-3.62	0.02-53.71	0.05-16.32
Length (Mean ± SD, mm)	2.38 ± 6.17	0.42 ± 0.50	1.67 ± 4.14	1.76 ± 2.12
Length ($mm \cdot mm^{-3}$)	20.21	24.17	23.43	13.67

3.5. The branching of dermal blood vessels

The branches of dermal blood vessels are complex. To better visualize the vascular structure, we tracked the blood vessels in the dermis and reconstructed them in 3D. The results showed that there were 44.59 branches in 1 mm^3 of FTD, 48.62 branches in 1 mm^3 of the PDP layer, 56.20 branches in the SRP layer, and 25.53 branches in the DRP layer **(Table 4)**. The mean number of branches per vessel was significantly higher in the SRP group than in the PDP group (Fig. 5b; 4.01 ± 13.49 *vs.* 0.84 ± 1.39, $p < 0.01$). However, there was no statistical difference between the SRP and DRP layers (Fig. 5b; 4.01 ± 13.49 *vs.* 3.28 ± 3.61, $p = 0.8485$), or between the PDP and DRP layers (Fig. 5b; 0.84 ± 1.39 *vs.* 3.28 ± 3.61, $p = 0.0934$). The branch number of each vessel ranged from 0 to 265 in FTD,

from 0 to 14 in the PDP, from 0 to 202 in the SRP, and from 0 to 27 in the DRP. A value of 0 indicated that the blood vessel had no branches **(Table 4)**. In Figures 5c and 5d, one representative blood vessel from 787 dermal vessels showed 179 generation points with a total of 265 branches. Another typical blood vessel showed 17 generation points with 41 branches **(Fig. 6e and 6f)**. These examples highlighted the considerable structural heterogeneity and hierarchical depth of the dermal vascular network.

Table 4. The number of branches of blood vessels in the different dermal layers

Parameter	**FTD**	**PDP**	**SRP**	**DRP**
Count	787	397	735	260
Branch /Vessel (Mean ± SD)	5.25 ± 18.96	0.84 ± 1.39	4.01 ± 13.49	3.28 ± 3.61
Branch range	0-265	0-14	0-202	0-27
Branch /mm³	44.59	48.62	56.20	25.53

FTD, full-thickness dermis; PDP, papillary dermal plexus; SRP, superficial reticular plexus;

DRP, deep reticular plexus.

3.6. The dermal blood vessels' morphological classes

A systematic classification of dermal blood vessels from a 3D view might provide more valuable information for histology and physiology. Thus, we analyzed the morphological features of 787 dermal blood vessels based on fractal dimension, tortuosity,

and average curvature, which reflected their branching richness and spatial intricacy. The results showed that the median values of fractal dimension, tortuosity, and average curvature were 1.069, 1.653, and 0.153 respectively **(sFig. 1)**. The vessels were first categorized as either complex or simple based on whether their fractal dimension exceeded the median value, to reflect branching complexity and spatial organization. Each category was further subdivided using the median values of tortuosity and curvature, yielding six distinct morphological vessel classes: simple-straight, simple-curved, simple-tortuous, complex-straight, complex-curved, and complex-tortuous **(Table 5)**.

Table 5. Threshold criteria for dermal vessels' morphological classification

Vascular Phenotype	Fractal Dimension	Tortuosity	Average Curvature
Complex-curved	> 1.069	> 1.653	> 0.153
Complex-tortuous	> 1.069	> 1.653	< 0.153
Complex-straight	> 1.069	<1.653	< 0.153
Simple-curved	< 1.069	> 1.653	> 0.153
Simple-tortuous	< 1.069	> 1.653	< 0.153
Simple-straight	< 1.069	<1.653	< 0.153

Among the six classes, complex-straight vessels (n = 199) and simple-straight vessels (n = 195) predominated **(Fig. 7d and 7g)**, which accounting for 50.1% of the total **(Table 6)**. Simple-tortuous vessels (n = 124) accounted for 15.8%, and complex-curved vessels (n = 116) accounted for 14.7% of the total **(Fig. 7b, f) (Table 6)**. Complex-tortuous vessels (n = 78) and simple-curved vessels (n = 75) accounted for the smallest fractions, i.e., 9.9% and 9.5%, respectively, of the total **(Fig. 7c and 7e) (Table 6)**. Moreover, the proportion of the 6 different classes of blood vessels was calculated for each dermal layer **(Table 7)**. In the PDP layer, there were a total of 397 blood vessels, of which straight blood vessels accounted for 46% (n = 184), with simple-straight blood vessels accounting for 43.8% (n = 174). The proportion of tortuous blood vessels was 36% (n = 141), with complex-tortuous blood vessels accounting for 28.5% (n = 113). The proportion of curved blood vessels was 18% (n = 72), and simple-curved blood vessels accounted for 16.6% (n = 66) **(Table 7)**. In the SRP layer, there were a total of 735 blood vessels: the straight blood vessel fraction amounted to 46% (n = 336), with simple-straight blood vessels accounting for 29.2% (n = 215). The proportion of tortuous blood vessels was 32% (n = 235), with complex-tortuous blood vessels accounting for 19.5% (n = 143). The proportion of curved blood vessels was 22% (n = 164), with simple-curved blood vessels accounting for 12% (n = 88) **(Table 7)**. In the DRP layer, there were a total of 260 blood vessels; the proportion of straight blood vessels was 50% (n = 130), with simple-straight blood vessels accounting for 30% (n = 78). The proportion of tortuous blood vessels was 29% (n = 75), with simple-tortuous blood vessels accounting for 17.7% (n=46). Finally, the fraction of curved blood vessels was 21% (n = 55), with complex-curved blood vessels accounting for 12.3% (n = 32) **(Table 7)**.

Therefore, the straight vessels, especially simple-straight vessels, were the prevailing types in the PDP, SRP and DRP, whereas curved vessels were the least frequent type.

Table 6. Morphometric characteristics of dermal vessels' classification groups

Vessel Type	Vessel Count	Fractal Dimension	Tortuosity	Average Curvature
Complex-curved	116	1.205 ± 0.090	3.355 ± 3.146	0.184 ± 0.024
Complex-tortuous	78	1.188 ± 0.099	3.327 ± 2.451	0.133 ± 0.017
Complex-straight	199	1.227 ± 0.144	1.121 ± 0.345	0.159 ± 0.030
Simple-curved	75	0.963 ± 0.070	5.678 ± 7.851	0.190 ± 0.030
Simple-tortuous	124	0.966 ± 0.062	7.480 ± 9.683	0.119 ± 0.021
Simple-straight	195	0.971 ± 0.066	1.213 ± 0.255	0.151 ± 0.041

Table 7. Distribution of vessel phenotypes in the different dermal layers

Vessel Type	PDP		SRP		DRP	
	Count	Proportion	Count	Proportion	Count	Proportion
Complex-curved	6	1.5%	76	10.3%	32	12.3%
Simple-curved	66	16.6%	88	12%	23	8.8%
Sum	72	18.1%	164	22.3%	55	21.1%
Complex-tortuous	113	28.5%	143	19.5%	29	11.2%
Simple-tortuous	28	7.1%	92	12.5%	46	17.7%
Sum	141	35.6%	235	32%	75	28.9%
Complex-straight	10	2.5%	121	16.5%	52	20%

Simple-straight	174	43.8%	215	29.2%	78	30%
Sum	184	46.3%	336	45.7%	130	50%

PDP, papillary dermal plexus; SRP, superficial reticular plexus; DRP, deep reticular plexus.

3.7. The course orientation of dermal blood vessels

The spatial configuration of dermal blood vessels could critically determine their functional specialization. A standardized coordinate system—X-axis (red, parallel to the skin surface), Y-axis (green, perpendicular to the skin surface), and Z-axis (blue, anterior-posterior parallel to the skin surface)— was used to analyze vascular course orientations **(Fig.8a-d)**.

The results showed that in the PDP layer, the average orientation along the Y-axis was 40.11° ± 25.91°, whereas that along the Z-axis was 62.55° ± 20.29°, indicating that the dermal blood vessels ran predominantly perpendicular to the skin surface. In the SRP layer, the angle between the vessels and the X-axis was 42.30° ± 25.88°, the angle between the vessels and the Z-axis was 58.75° ± 21.14°. In the DRP layer, the angle between the vessels and the X-axis was 42.26° ± 26.05°, the angle between the vessels and the Z-axis was 58.02° ± 21.06° **(Table 8; Fig. 8e-g)**. Interestingly, along both the horizontal Z-axis (anterior–posterior) and the X-axis (left-right), the vessels running parallel to the skin surface

predominated in the SRP and DRP layers. The horizontally distributed vascular network can cover a wider range of skin areas, enabling more uniform blood supply to structures such as the epidermis, hair follicles, and sweat glands. This ensures adequate nutrient and oxygen supply, while effectively removing metabolic waste products.

Table 8. 3D orientation metrics of dermal vessels

Layer's Plexus	Angle to X-axis (°)	Angle to Y-axis (°)	Angle to Z-axis (°)
PDP	43.55 ± 25.97	40.11 ± 25.91	62.55 ± 20.29
SRP	42.30 ± 25.88	49.48 ± 26.33	58.75 ± 21.14
DRP	42.26 ± 26.05	47.52 ± 25.89	58.02 ± 21.06

FTD, full-thickness dermis; PDP, papillary dermal plexus; SRP, superficial reticular plexus; DRP, deep reticular plexus.

4.Discussion

In this study, we successfully revealed the 3D architecture of adult human dermal blood vessels by using a stereo tissue imaging technique, which integrates specialized methods to induce skin tissue transparency with state-of-the-art image processing technologies. This study quantitatively measured the vessel lengths, branches, inner diameters, and angular orientations at the unprecedented axial resolution of 1.0 μm. Based on these data, we estimated the total length, potential volume, and inner surface area of the dermal blood vessels throughout the whole adult human body. Therefore, this work

provided novel and fundamental data that could significantly improve our understanding of the physiological as well as pathological activities occurring within skin tissue.

It is well established that the blood vessel diameter critically determines blood volume potential and functional indications. Previous studies showed that, in the forearm skin, the inner endothelial tube diameter of arterial capillaries ranges from 4 to 6 μm[14], while that of postcapillary venules ranges from 8 to 26 μm, and that of postcapillary venules in the papillary dermis varies from 10 to 15 μm[15]. However, such studies clearly had several flaws, such as the limited precision of the 2D measurements, and the difficulty distinguishing the open from the closed status of the vessels. The presently used method can trace blood vessels and overcome the potential impact of 2D slicing direction or angle on diameter measurements. As shown in Table 2, the dermal blood vessel diameters ranged from 0.01 μm to 74 μm; these values are much greater than those previously reported. Moreover, in the PDP layer the dermal blood vessel diameters were quite narrow (i.e., from 0.23 to 8.41 μm); again, such values were much smaller than those found in earlier reports[14,15]. One of the most interesting findings was the open-closed status of dermal blood vessels. Approximately 88.88% of the latter ones in the PDP layer, 44.51% in the SRP layer and 45.76% in the DRP layer were closed. These results indicated the variability in the dermal strata demands for nutrition and oxygen. We also noted that most of the open dermal blood vessels were located around skin appendages **(sFig. 2)**, which proved the intense metabolic needs of these active biounits. Consequently, comparative studies examining the open-closed status of dermal blood vessels around the appendages in conditions such as acne and alopecia could be clinically valuable.

Another interesting issue is the dermal vessels' length. One 2D study reported that in a 4-mm² area of the forearm at depths of 40–440 μm below the skin surface, the vascular network length was 12.3 ± 1.7 mm in young subjects and 11.1 ± 2.0 mm in older subjects [16]. By means of non-invasive video-capillaroscopy, Li L et al. showed that in a 1.73 mm² area of the crow's feet, 1–1.5 mm below the skin surface, the maximal skin vessel length was 3.41 mm, whereas the shortest (on the hand back) one was 1.08 mm[17]. Our results showed that within a 1 mm³ volume of abdominal dermis the blood vessels' total length was 20.21 mm. However, the number and the length of the dermal blood vessels differed in the diverse dermal layers. As shown in Table 4, the highest number of vessels was in the PDP stratum, i.e., 58 blood vessels in 1 mm^3, while the averaged maximal length of individual dermal blood vessel was 1.76 mm in the DRP layer, while the vessels' largest total length, i.e., 24.17 mm, was located in the PDP layer. Because the sites (face, limbs *vs*. abdomen), depths (0.440 mm, 1.5 mm, *vs*. 5.25 mm), and the methods used (2D *vs*. 3D) in our study differed from those reported by earlier works, it is reasonable that our results were dissimilar. However, we believe that data based on the 3D measurement approach should be more precise, as the 2D technique could not take into account the Z-axis (depth) variations, and the loss of substantial amounts of tissue components during the slicing procedure, which would consistently cause a consistent underestimation of the actual vessels' length. The 3D tissue imaging technique better preserves the microstructure of tissues and enables 1.0 μm precision measurements, thus yielding data of higher accuracy and greater precision. Therefore, we estimated the total length of dermal blood vessels based on data gained from 1 mm^3 of dermal tissue, which was estimated to be from 36.4 to 181.9 km (see part 4 of the Results). In the past, few studies focused on the length of

microvessels. The most well-known study based on muscle tissue HE staining was conducted 100 years ago; in it the author proposed that the total length of human blood vessels was 96,000-100,000 km [18]. According to our present data on the dermis, it is reasonable to posit that the figure of 96,000-100,000 km in length needs to be revised.

Currently, the accurate assessment of dermal blood vessel volume remains a scientific challenge. Relative changes in skin blood flow and volume are primarily estimated using cardiac output assessments and spectroscopic measurements[19, 20]. So far, no study has reported the total dermal vessel volume of the whole body. To address this issue, we calculated the dermal vessel volume (DVV) based on the inner diameters and lengths. As the data about the vessel inner diameters were not normally distributed, we used the median value of inner diameters. Our results showed that under normal conditions, in which about 49% of dermal blood vessels were closed, the median inner diameters were 2.8 μm in the PDP, 3.45 μm in the SRP, and 3.45 μm in the DRP. Therefore, for an adult patient (170 cm ,70 kg) with a total skin surface area of 1.8 m², under general anesthesia (GA), the DVV-GA, based on the average median diameter, was only 0.8 ml. The dermal vascular volume was relatively small. This is related to dermal vasoconstriction caused by the thermoregulatory defense response during general anesthesia. Besides, this provided a good explanation for the increase in the incidence of pressure ulcers among adults undergoing surgery[21,22]. On the other hand, based on a condition in which vessels were fully open and dilated, the DVV-max was 412.0 ml, which indicated a potentially huge pool and role in critical situations, such as severe sepsis.

The inner (or interfacial) surface area (ISA) of blood vessels is especially important in materials exchange. Hitherto, no data on dermal blood vessel ISA had been reported. We

found that under physiological conditions a 70-kg, 170-cm-tall adult with a dermal thickness ranging from 1 mm to 5 mm might have a total body ISA of 0.39 to 1.97 m^2. Of this, the PDP layer's total ISA was 0.13 m^2, accounting for 7% of the total ISA of dermal blood vessels. The SRP layer's total ISA was 1.21 m^2, accounting for 62% of the total ISA. The DRP layer's total ISA was also 0.60 m^2, accounting for the remaining 31% of the total. From these data we could deduce that, although the PDP layer represented only 7% of the total ISA of dermal blood vessels, its ISA per 1 mm^3 volume reached up to 0.213 mm^2. This reflects the PDP layer blood vessels' unique structure, which exerts their physiological functions by maximizing efficiency within a limited space. Compared to the other two strata, the SRP layer exhibited the highest ISA values both per unit volume (0.254 $mm^2.mm^{-3}$) and in total proportion, indicating that it might be the primary region for the exchange of materials. In the DRP layer, although the tissue volume was close to the SRP layer's, the ISA per 1 mm^3 volume was only 0.148 mm^2, indicating that its function focused on blood flow rather than materials exchange. In addition, were the dermal blood vessels fully dilated in a standard size adult human, the potential ISA would be approximately 28.86 m^2, which is 15-fold greater than that under normal physiological conditions. In summary, the quantification of dermal blood vessels' ISA could help clarify their physiological functions as well as enhance vasoactive drug delivery.

The branching structure of blood vessels reflects the complexity of the microcirculation network. Hitherto, the highest reported generation number of human vascular branches has come from a micro-CT analysis of the renal artery [23]. This study reported a total of main renal artery 26 branch generations from the renal hilum to the glomerular afferent arteriole. Regarding the generation of skin vascular branches, Geyer et

al. used high-resolution episcopic microscopy to observe detailed images of the thumb pad skin cover. They observed 5–11 branches of cutaneous arteries within a 2739×2054×3000 μm^3 area that included the epidermis, dermis, hypodermal-dermal junction, and the most superficial parts of the hypodermis[24]. In the present study, we could trace dermal blood vessel branches up to 179 generations within a 9810 ×1800 × 5250 μm^3 volume composed exclusively of dermal tissue. These data revealed how complex the network of dermal blood vessels is.

With the development of tissue clearing and image reconstruction techniques, it became possible to clearly visualize the 3D vascular trajectory of individual dermal vessels. Based on the complexity of their branching patterns and spatial trajectories, six types of dermal blood vessels could be classified according to fractal dimension, tortuosity, and average curvature[25]. Tortuous vessels increase the effective length of vessels within a confined space[26], whereas straight vessels lower vascular resistance, thereby facilitating blood flow and nutrient delivery. A reduction in tortuous vessels indicating a diminished tissue demand and may reflect skin aging and a heightened risk of ulcers[27-29]. In the SRP layer, complex-tortuous and simple-straight vessel types predominated, indicating that longer tortuous vessels met the functional requirements of the SRP in substance exchange, while straight vessels shortened the transport distance, facilitating blood flow regulation and thermoregulation. In the DRP layer, complex-straight and simple-straight vessel types predominated, indicating that straight vessels reduced the blood flow resistance to fulfill the function of the DRP in blood transport and temperature regulation. By contrast, complex-tortuous and simple-straight vessel types predominated in the PDP layer, suggesting that tortuous vessels increased the contact surface between blood and tissue to

ease material exchange, whereas straight vessels decrease flow resistance to help remove metabolic waste. From a 3D perspective, skin vessels exhibit a dendritic distribution pattern as they extend from the deep dermis toward surrounding tissues. This means that vessels not only run superficially but also ascend from the deeper dermal zone. It was also noted that vessels in the PDP layer tended to run vertically, whereas they ran horizontally in the DRP and SRP layers **(Fig. 9)**.

It should be pointed out that the data in this study were sourced from a single skin sample from one abdominoplasty patient. Although this limits the generalizability, it provides a foundation for future studies with larger sample sizes. Going forward, we will also analyze additional skin samples as well as the different parts of the body and different ages to explore the characteristics of dermal blood vessels, thereby contributing to a better understanding of dermal blood vessels.

5. Conclusion

In this study, for the first time, we precisely constructed a 3D map of human dermal microvessels based on quantitative data about their inner diameters, 3D trajectories, branch numbers, course angles, and segments lengths. We also calculated human dermal vessel length, surface area, and potential volume by means of tissue clearing techniques and digital image processing systems. These findings overturn long-held dogmata and fundamentally recalibrate our understanding of skin vascular system. This precise 3D quantitative method and precise measurement of microstructures might provide a new perspective to better understand vascular physiology and the pathogenesis of certain diseases, potentially improving diagnosis and prognosis in the future.

Declaration of Competing Interest

There are no conflicts of interest listed by the authors.

Acknowledgments

This work was supported by National Key Research and Development Program (2002YFC2403101); Shenzhen Portion of Shenzhen-Hong Kong Science and Technology Innovation Cooperation Zone, (project No. HTHZQSWS-KCCYB-2023060); Medical Engineering Interdisciplinary Research Fund Project of Shenzhen University(project No. 2023YG017); National Natural Science Foundation of China (General Program, grant No. 82472545); National Natural Science Foundation of China(Youth Program,grant No.82402929); National Natural Science Foundation of China(Youth Program,grant No.82402949); Zunyi Municipal Science and Technology Programme Project (2025)291; Guizhou Provincial Department of Science and Technology Basic Research Programme (2025); Guizhou Science and Technology Cooperation Basic MS (2026) 946.

References

1. Matienzo D, Bordoni B. Anatomy, Blood Flow. In: StatPearls. Treasure Island (FL): StatPearls Publishing; July 25 (2023).

2. Zhang H, Wu C. 3D printing of biomaterials for vascularized and innervated tissue regeneration. Int J Bioprint. 2023;9(3):706. doi:10.18063/ijb.706.

3. Nguyen JD, Duong H. Anatomy, Shoulder and Upper Limb, Veins. In: StatPearls. Treasure Island (FL): StatPearls Publishing; August 14, 2023.

4. Liu YH, Brunner LM, Rebling J, et al. Non-invasive longitudinal imaging of VEGF-induced microvascular alterations in skin wounds. Theranostics. 2022;12(2):558-573. doi:10.7150/thno.65287.

5. Liu P, Zhang T, Huang Y. Three-dimensional model of normal human dermal tissue

using serial tissue sections. Front Bioeng Biotechnol. 2024;12:1347159. doi:10.3389/fbioe.2024.1347159.

6. Yi Y, Li Y, Zhang S, et al. Mapping of individual sensory nerve axons from digits to spinal cord with the transparent embedding solvent system. Cell Res. 2024;34(2):124-139. doi:10.1038/s41422-023-00867-3.

7. Jing D, Zhang S, Luo W, et al. Tissue clearing of both hard and soft tissue organs with the PEGASOS method. Cell Res. 2018;28(8):803-818. doi:10.1038/s41422-018-0049-z

8. Yu T, Zhong X, Li D, Zhu J, Tuchin VV, Zhu D. Delivery and kinetics of immersion optical clearing agents in tissues: Optical imaging from ex vivo to in vivo. Adv Drug Deliv Rev. 2024;215:115470. doi:10.1016/j.addr.2024.115470

9. Ni Y, Wu J, Liu F, et al. Deep imaging of LepR+ stromal cells in optically cleared murine bone hemisections. Bone Res. 2025;13(1):6. doi:10.1038/s41413-024-00387-9

10. Jing D, Zhang S, Luo W, et al. Tissue clearing of both hard and soft tissue organs with the PEGASOS method. Cell Res. 2018;28(8):803-818. doi:10.1038/s41422-018-0049-z

11. Molbay M, Kolabas ZI, Todorov MI, Ohn TL, Ertürk A. A guidebook for DISCO tissue clearing. Mol Syst Biol. 2021;17(3):e9807. doi:10.15252/msb.20209807.

12. Wang H, Zhu Q, Ding L, et al. Scalable volumetric imaging for ultrahigh-speed brain mapping at synaptic resolution. Natl Sci Rev. 2019;6(5):982-992. doi:10.1093/nsr/nwz053.

13. Berg S, Kutra D, Kroeger T, et al. ilastik: interactive machine learning for (bio)image analysis. Nat Methods. 2019;16(12):1226-1232. doi:10.1038/s41592-019-0582-9

14. Yen A, Braverman IM. Ultrastructure of the human dermal microcirculation: the horizontal plexus of the papillary dermis. *J Invest Dermatol*. 1976;66(3):131-142. doi:10.1111/1523-1747.ep12481678

15. Braverman IM. The cutaneous microcirculation. J Investig Dermatol Symp Proc. 2000;5(1):3-9. doi:10.1046/j.1087-0024.2000.00010.x.

16. Wang-Evers M, Casper MJ, Glahn J, et al. Assessing the impact of aging and blood pressure on dermal microvasculature by reactive hyperemia optical coherence tomography angiography. Sci Rep. 2021;11(1):13411. doi:10.1038/s41598-021-92712-z.

17. Li L, Mac-Mary S, Sainthillier JM, Nouveau S, de Lacharriere O, Humbert P. Age-related changes of the cutaneous microcirculation in vivo. Gerontology. 2006;52(3):142-153. doi:10.1159/000091823

18. August Krog. The Capillary Blood-Vessels. Nature. 66,2808:270-272 (1922).

19. Hall, J. E., & Hall, M. E. Guyton, and Hall Textbook of Medical Physiology (14th ed.). Elsevier Health Sciences. ISBN: 978-0323640039 (2020).

20. Jacques SL. Optical properties of biological tissues: a review. Phys Med Biol. 2013;58(11):R37-R61. doi:10.1088/0031-9155/58/11/R37.

21. Kurian S, Moore Z, Patton D, George S. The Incidence of Pressure Ulcers in Surgical Patients: A Systematic Review. Int Wound J. 2025;22(8):e70738. doi:10.1111/iwj.70738.

22. Kim JM, Lee H, Ha T, Na S. Perioperative factors associated with pressure ulcer development after major surgery. Korean J Anesthesiol. 2018;71(1):48-56. doi:10.4097/kjae.2018.71.1.48

23. Rahmani S, Jafree DJ, Lee PD, et al. Mapping the arterial vascular network in an intact human kidney using hierarchical phase-contrast tomography. Npj Imaging. 2025;3(1):39. doi:10.1038/s44303-025-00090-2.

24. Geyer SH, Nöhammer MM, Tinhofer IE, Weninger WJ. The dermal arteries of the human thumb pad. J Anat. 2013;223(6):603-609. doi:10.1111/joa.12113

25. Wu L, Gong X, Wang W, et al. Association of retinal fractal dimension and vessel tortuosity with impaired renal function among healthy Chinese adults. Front Med (Lausanne). 2022;9:925756. doi:10.3389/fmed.2022.925756.

26. Carraro M, Negandhi J, Kuthubutheen J, et al. Attenuating Cardiac Pulsations within the Cochlea: Structure and Function of Tortuous Vessels Feeding Stria Vascularis. ISRN Otolaryngol. 2013;2013:941757. doi:10.1155/2013/941757.

27. Zhou S, Li Z, Li X, et al. Crosstalk between endothelial cells and dermal papilla entails hair regeneration and angiogenesis during aging. J Adv Res.2025;70:339-353. doi:10.1016/j.jare.2024.05.006.

28. Chen J, Sivan U, Tan SL, et al. High-resolution 3D imaging uncovers organ-specific vascular control of tissue aging. Sci Adv. 2021;7(6):eabd7819. doi:10.1126/sciadv.abd7819.

29. Vélez González JJ, Berger M, Schiele S, et al. Dynamic optical coherence tomography of chronic venous ulcers. J Eur Acad Dermatol Venereol. 2024;38(1):223-231. doi:10.1111/jdv.19496.

Figure captions

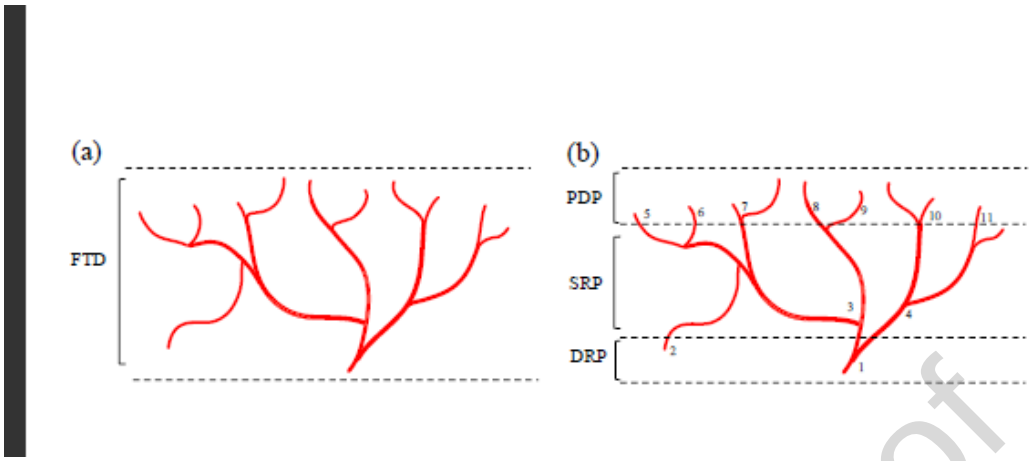

Fig.1. Schematic diagram of vessel counting method. (a) When calculating full-thickness dermal vessels, one vessel extending through the full thickness of the dermis is counted as one vessel. **(b)** The same vessel, when calculating the number of layered vessels, can be divided into 11 vessels. FTD, full-thickness dermis; PDP, papillary dermal plexus; SRP, superficial reticular plexus; DRP, deep reticular plexus.

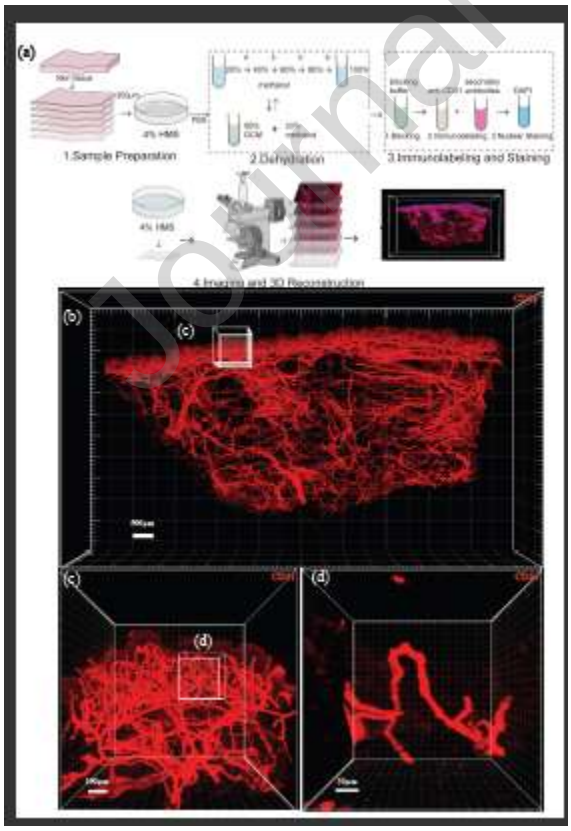

Fig. 2. Operative procedures and image displays of the dDISCO-HMS technique. (a) Schematic diagram of transparent human abdominal skin obtained using the dDISCO-HMS technique. **(b)** 3D view of dermal tissue (blue, DAPI) and vascular network (red, CD31) from the papillary layer to the deep reticular layer. The boxed region is magnified in (c). **(c)** Vascular structure of the dermal papillary layer and the superficial reticular plexus. Boxed region indicates the magnified view in (d). **(d)** Vascular structure of the dermal papillary layer visualized in 3D at 1.0 μm resolution, revealing capillary loops. Scale bars: (b) 500 μm, (c) 90 μm, (d) 30 μm. DCM, dichloromethane; HMS, hydrogel-based matrix stabilization.

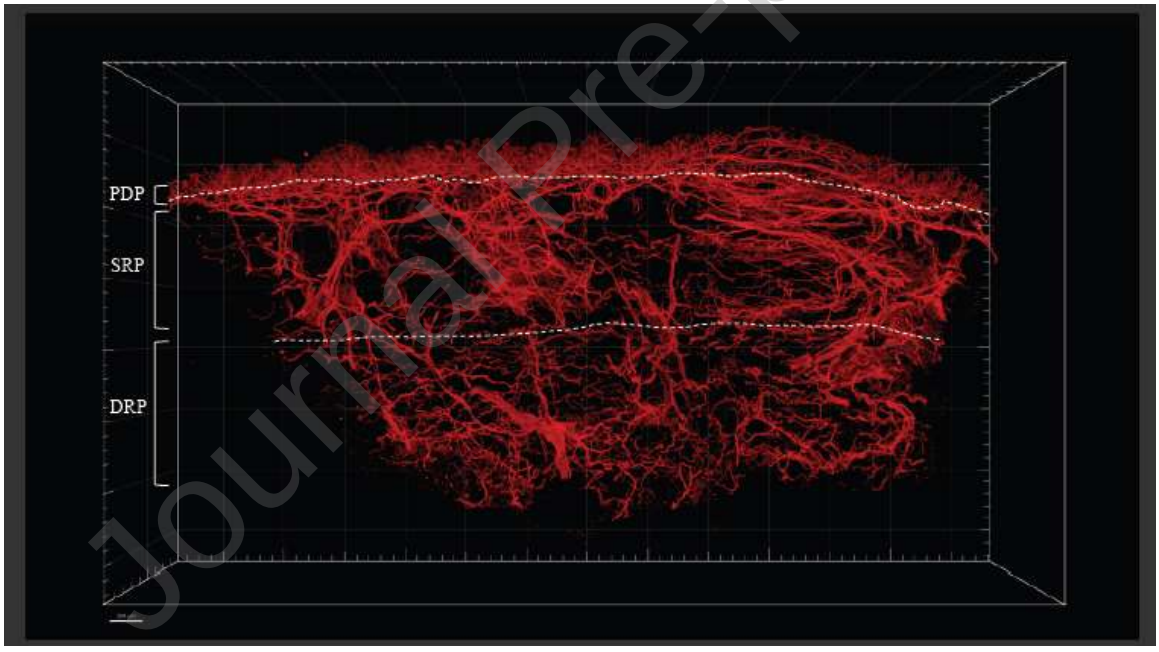

Fig.3. Schematic diagram of dermal blood vessel plexuses. The immunostained (CD31) dermal vasculature is organized into three distinct plexuses based on histological depths. White dashed lines demarcate the boundaries of the papillary dermal plexus (PDP), superficial reticular plexus (SRP), and deep reticular plexus (DRP). Scale bar: 500 μm.

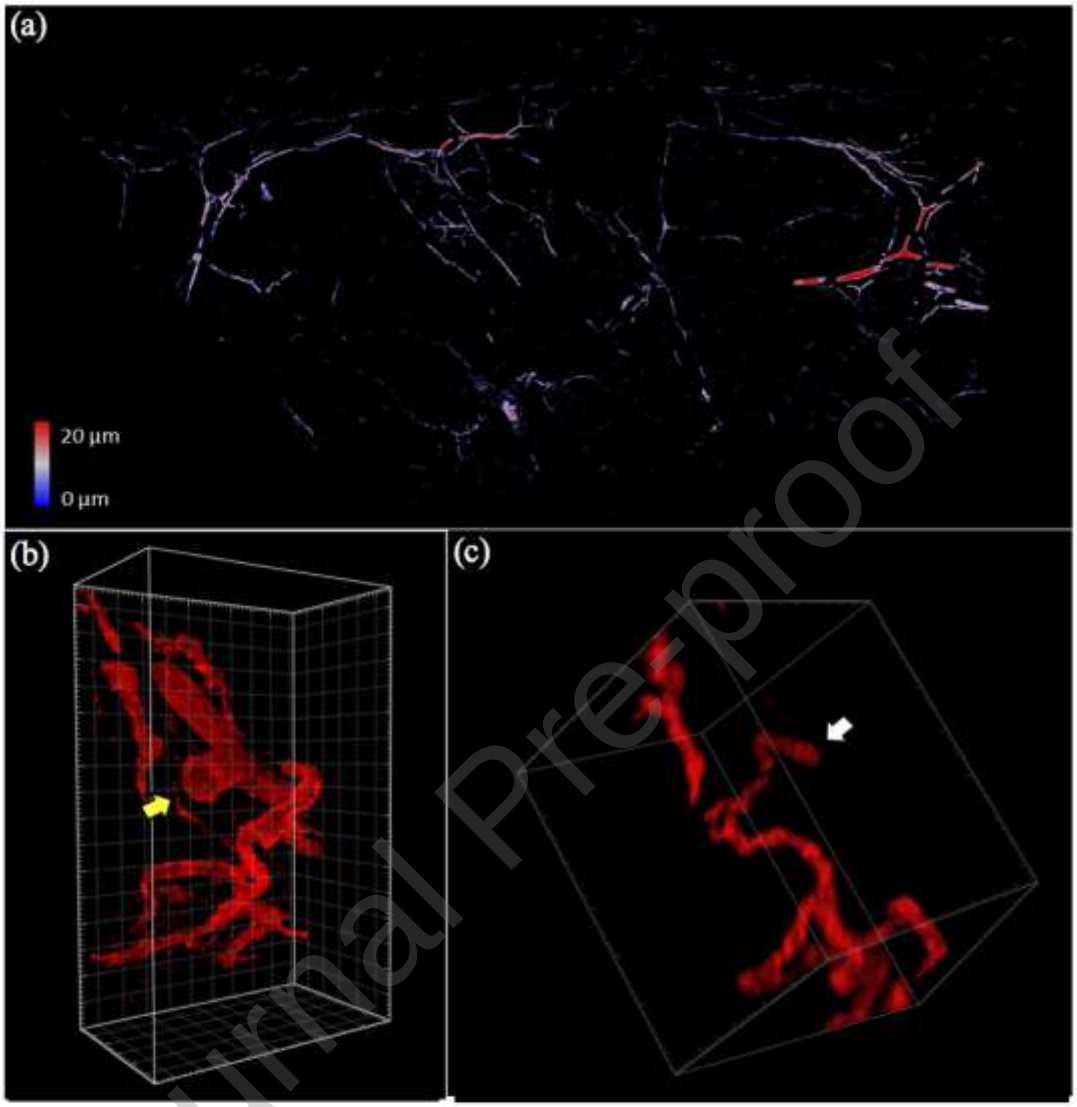

Fig. 4. Open and closed dermal vessels. (a) Pseudo-color display of open and closed dermal blood vessels. Red color represents the largest inner diameter (> 20 μm), while blue color reveals the smallest ones (0.0 μm). **(b)** Representative image of an open vessel with weak or absent fluorescence staining inside its lumen (yellow arrow). **(c)** Representative image of a closed solid-cable-like vessel (white arrow).

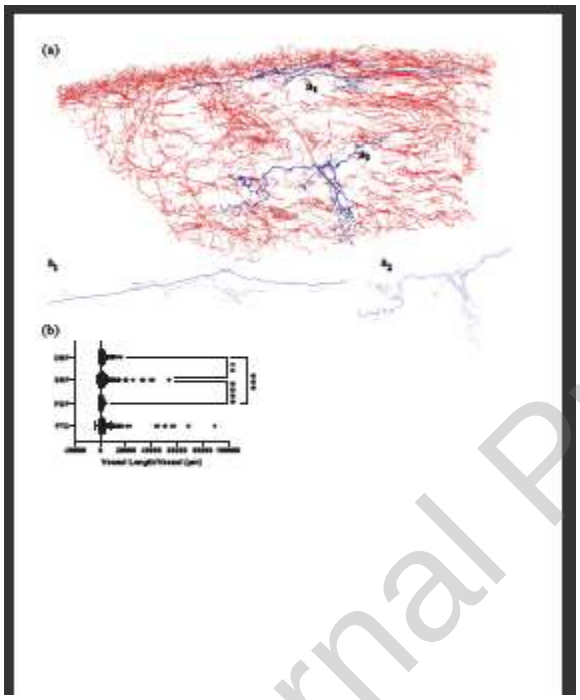

Fig. 5. 3D reconstruction and segmentation of dermal vascular networks. (a) Representative 3D view of the dermal microvasculature. Two typical dermal blood vessels (a_1, a_2) have been traced using Connected Soma-Working-Cable (SWC) nodes. a_1 and a_2 each correspond to a single vessel extracted from the microvascular network. (b) Violin plots showing the distribution of vessel-segment lengths across the full-thickness dermis (FTD) and its individual layer plexuses (PDP, SRP, DRP). Statistical significance was assessed using one-way ANOVA and post hoc test (***$p < 0.001$, ****$p < 0.0001$).

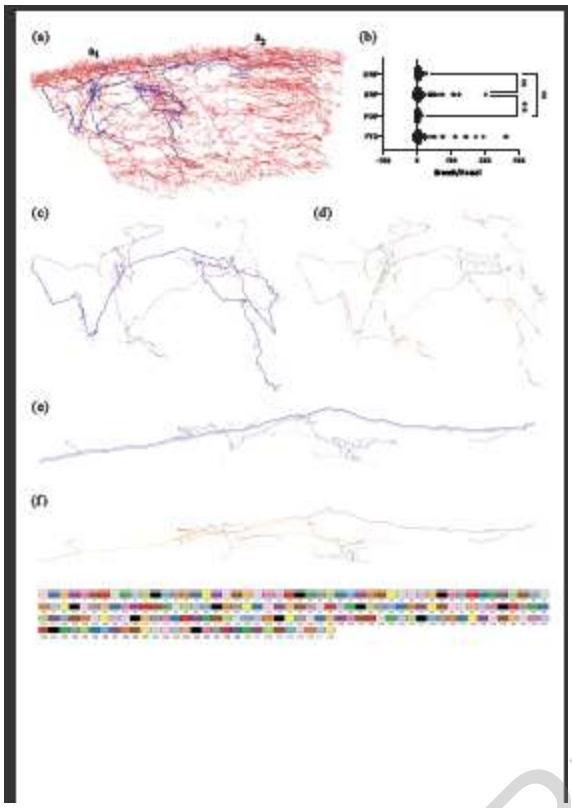

Fig. 6. The reconstruction of dermal blood vessel branches and single vessel trajectory mapping. (a) 3D projection of the entire dermal vascular network showing its depth-resolved organization. The blood vessel trunks and branches were distinguished by color values and line thicknesses. Darker colors with thicker lines indicated the blood vessels trunks, while lighter colors with thinner lines marked vessel branches. Two representative single vessels (a_1, a_2) were traced for branch and trajectory analysis. (b) Violin plots show the distribution of branch counts across full-thickness dermis (FTD) and individual layers' plexuses (i.e., PDP, SRP, DRP). (c) The magnified single blood vessel a_1 was extracted from the microvascular network. The red dots represent the origin points of the 265 branches of this blood vessel. **(d)** This skeletonized reconstruction of individual vessels' trajectories, color-coded by segment identity, illustrates the morphologically distinct branching characteristics of the dermal blood vessels. The representative dermal blood

vessel (a_1) shows 179 branch generation points. **(e)** Another typical dermal blood vessel (a_2) showed 41 branches and **(f)** 17 generation points. The heatmaps depict the segmental assignments across the entire vascular network. Statistical significance was determined by one-way ANOVA and post hoc test (**$p < 0.01$).

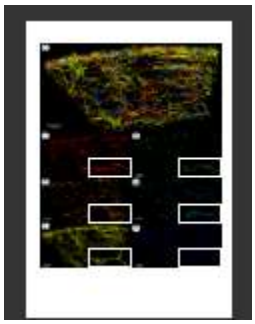

Fig. 7. The morphological classes of dermal blood vessels. (a) Representative image of the merged vascular networks across all dermal strata. **(b–g)** Schematic illustrations of the six vessel phenotypes as classified according to tortuosity, curvature, and fractal dimension: **b**, Complex-curved; **c**, Complex-tortuous; **d**, Complex-straight; **e**, Simple-curved; **f**, Simple-tortuous; **g**, Simple-straight. The phenotypes distribution shows a depth-dependent specialization, reflecting a layer-specific balance between hemodynamic efficiency and structural complexity. All scale bars: 1 mm.

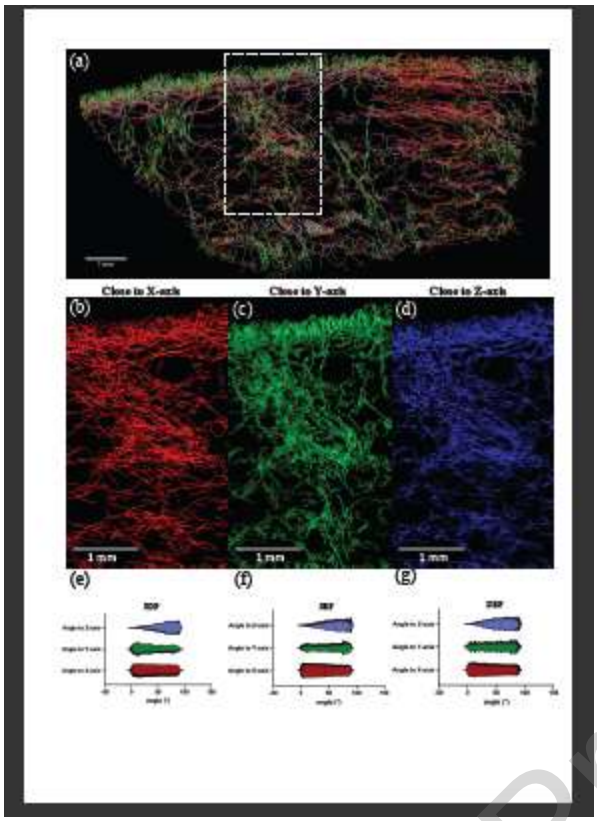

Fig. 8. Orientation of dermal blood vessel courses in different layers. (a) Merged view of vascular networks and vessel orientation across all dermal strata. 3D reconstruction of the human dermal microvasculature after pseudo-colored according to the local vessel course orientation related to the global coordinate axes indicated in the text. The white dashed-line region indicates the corresponding magnified views in (b), (c), and (d). **(b)** Vessel orientation close to the X-axis (red); **(c)** Vessel orientation close to the Y-axis (green); **(d)** Vessel orientation close to the Z-axis (blue). **(e–g)** Violin plots showing the quantifications of vessel course orientation angles relative to the X-, Y-, and Z-axes in the PDP **(e)**, SRP **(f),** and DRP **(g)**. All scale bars: 1 mm.

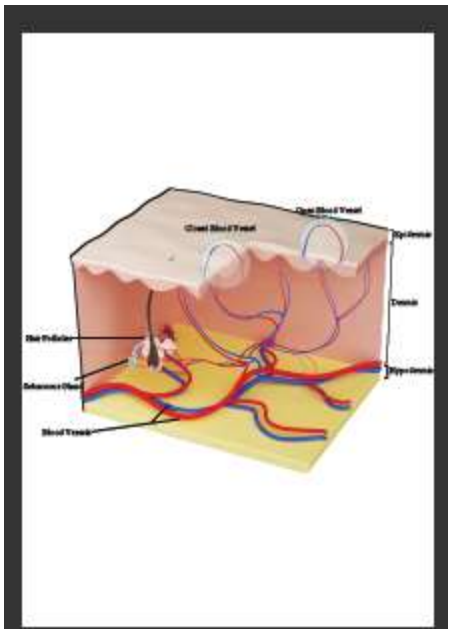

Fig. 9. Mesoscale 3D schematic representation of microvessels in human skin. In a 3D perspective, dermal blood vessels exhibited a dendritic distribution pattern as they extended from deep to superficial layers of the dermis. In the deep layer of the dermis, vessels mainly ran horizontally, while they mainly ran vertically in the superficial stratum of the dermis. Moreover, while extending from deep to superficial layers, retrograde branches were emitted which run toward deeper tissues. Almost half of dermal vessels were either open or closed.

Ethics declaration

Informed consent and patient details

Written informed consent to take part in the study and to publish the article has been obtained from all participants or their legal representatives. The privacy rights of participants have been observed.

Human and biological material

This study included organ or tissue donors.

This study includes human biological material and consent was obtained by donors, or their next of kin or legal representatives, for use in this study and for publication of the article. The samples used in this research were not sourced from executed prisoners or prisoners of conscience.

Studies in Human

This study was performed in compliance with relevant laws, regulatory frameworks and guidelines where the research took place.

This study was approved by the Ethics Committee of the First Affiliated Hospital of Shenzhen University.

(Approval No. #2023-241-01PJ)

Declaration of Competing Interest

The authors declare that they have no known competing financial interests or personal relationships that could have appeared to influence the work reported in this paper.